Novel Multifunctional Optical-Fiber Probe: I. Development and Validation

Jinzhong Liu, John R. Grace, and Xiaotao Bi
Dept. of Chemical and Biological Engineering, The University of British Columbia, Vancouver, Canada V6T 1Z4

By combining aspects of optical fiber probes used to determine local particle concentrations and local particle velocities and by rapid signal processing, it is shown that a single probe can determine local instantaneous particle fluxes. Providing a transparent cover to prevent a "blind zone" is shown to be critical in improving the probe performance and linearity. A simple mechanistic model is successful in predicting the performance of the optical system. The results of the probe are validated using particles glued onto both a rotating disk and a flat vibrating surface.

Introduction

In gas−solids flow systems such as circulating fluidized beds (CFB) and pneumatic transport systems, local solids concentrations, particle velocities, and particle mass fluxes are important when characterizing hydrodynamics. Fundamental models, for example, CFD models for multiphase systems also require experimental validation. Obtaining accurate measurements is difficult given such factors as the lack of transparency of the particles, their erosive nature, their variability in size and shape, and the fluctuating nature of the flow.

Simultaneous measurement of particle concentration and velocities could provide important information on solids flow dynamics. In particular, the local instantaneous particle flux $G_s(t)$, is given by

$$G_s(t) = \rho_p v_p(t)[1 - \epsilon(t)]. \qquad (1)$$

For steady-state conditions, the time-average solids flux can be determined by integrating $G_s(t)$ over an extended time period, T, as

$$\overline{G_s} = \frac{1}{T}\int_0^T G_s(t)\,dt = \frac{\rho_p}{T}\int_0^T v_p(t)[1 - \epsilon(t)]\,dt. \qquad (2)$$

Solids sampling probes inserted and bent to face the flow, operated in an isokinetic or nonisokinetic mode, have been widely used to measure local time-average solids fluxes in CFB risers. However, this method cannot give instantaneous solids flux information, and, as discussed elsewhere (Liu, 2001), is not very accurate for highly turbulent (such as locally reversing) flows.

In CFB risers the time-average flux is in general not equal to the product of the time-average velocity and time-mean bulk density (Bi et al., 1996), that is

$$\overline{G_s} \neq \rho_s \overline{v_p}(1 - \overline{\epsilon}). \qquad (3)$$

This occurs because fluctuations in solids concentration are strongly correlated with fluctuations in particle velocity. Hence, errors are introduced if one tries to obtain one of these time averages from the other two, that is, by assuming an equality sign in Eq. 3. Simultaneous measurement of local instantaneous particle concentration and velocity also makes possible the determination of the Reynolds stress components of solids motion (Bao et al., 1996).

Although various experimental methods have been employed to measure solids concentration and particle velocity, as listed in Table 1, few of these techniques/combinations permit simultaneous determination of both parameters. Optical-fiber methods are most promising for this purpose.

Chrisman et al. (1994) developed a "backscattered particle imaging" (BPI) probe for *in situ* determination of particle concentration and velocity. Cocco et al. (1995) improved this probe by making the illuminating and light-collecting fibers converge toward each other. The particle velocity was determined by computing a derivative of the signal waveforms with respect to time, normalizing the derivative with respect to concentration, and multiplying the normalized derivative by a

Table 1. Summary of Local Particle Concentration and Velocity Measurement Techniques

	Local Solids Concentration	Local Particle Velocity	Comments
Pitot tube	No	Yes	Intrusive; inaccurate; easily blocked by fine particles; time-average only
X-ray or γ-ray transmission	Yes	No	High cost; limited by column dimensions; nondisturbing
Laser-Doppler anemometry	No	Yes	Limited to low solids concentrations; nonintrusive; high accuracy
Photographic and video techniques	Yes	Yes	Gives more information; easy to use; data analysis tedious and difficult; difficult to measure the interior region of the bed; not very accurate
Optical-fiber probe	Yes	Yes	Slightly intrusive; limited to low temperatures; simple to use; high accuracy; somewhat imprecise measuring volume
Capacitance probe	Yes	No	Intrusive; imprecise measuring volume

calibration constant. The probe was claimed to work well for solids volume concentrations up to 50%, but few experimental results were given to justify the method. Whether or not instantaneous and continuous concentrations and velocities could be obtained is also unclear.

Using two pairs of optical fibers, one above the other separated by 8 mm, Kallio (1996) simultaneously measured local voidages and particle velocities in a 7.3-m-high CFB riser of 0.25×1.0 m cross section, with sand of surface-volume mean diameter 230 μm as the particulate material. Ten measurements were obtained at $U_g = 3.97$ m/s, $G_s = 30.4$ kg/m²s for each measurement location. Although the results gave information on the order of magnitude of various properties, no instantaneous information was presented. Furthermore, the separation distance between pairs of 8-mm-dia. fibers appears to have been too large for Geldart type A (such as fluid catalytic cracking (FCC)) particles.

By combining and synchronizing the output of a laser Doppler velocimeter (LDV) and a phase Doppler particle analyzer (PDPA), Bao et al. (1996) measured the local instanta-

neous density and velocity components of a particle cloud. However, measurements were limited to spherical particles and very dilute suspensions, with solids volume fractions only of order 0.1%.

A two-channel single-fiber reflection (SFR) probe was developed by Werther et al. (1996). It is able to measure both local solids concentrations and instantaneous particle velocities. This probe has a limited solids voidage measurement volume, and the measured mean particle velocities were in close agreement with those measured by a laser Doppler anemometer (LDA) in the upper dilute zone of a circulating fluidized bed ($1 - \epsilon_m = 0.012$). No results were reported for denser suspensions, nor were attempts made to determine local instantaneous solids fluxes.

Currently, there is no method reported to measure ϵ and v_p in a synchronized simultaneous manner allowing determination of $G_s(t)$ for a wide range of suspension densities (such as $1 - \epsilon_m > 0.1$). Development of such a method was the goal of this study.

Fundamentals of Optical-Fiber Technique

Because of their simplicity, high accuracy, and relatively low cost, optical-fiber probes have been widely used in recent years to determine local solids concentrations and velocities in CFB risers. The measurements are usually based either on forward light scattering between emission and detection fibers separated by a short distance, or on backscattering to an optical-fiber system, with the projecting and receiving fibers intermingled or arranged in rows. Here we are interested only in the backscattering method, which is less intrusive.

Optical probes for measuring particle concentrations can be divided into two categories, depending on the relative sizes of the particles and probe, as shown in Figure 1. If the particle diameter is significantly smaller than the probe diameter (type I), all particles within the dotted circle in Figure 1 are detected. The integrated photomultiplier voltage can be correlated with the instantaneous concentration of particles using a suitable calibration procedure.

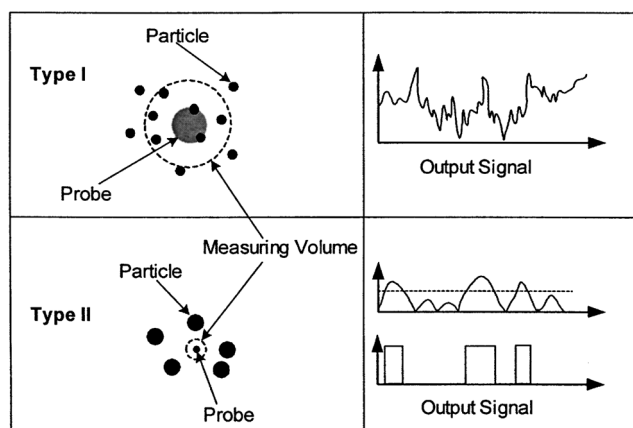On the other hand, when the particle diameter > the diameter of the optical probe (type II), single particles are de-

Figure 1. Types of optical probes.

Type I: $d_p \ll$ probe diameter; detection of swarm of particles; type II: $d_p >$ probe diameter; detection of single particles one at a time.

tected and the output from the light receiver is a series of pulses. The pulse count in a given time interval corresponds to the number of particles, and this can be converted to particle concentration, if the particle velocity is known. To achieve high accuracy, a long measuring time is needed and only time-average concentrations can be obtained using this option.

Various configurations of optical fibers have been explored (Chrisman et al., 1994; Werther et al., 1996; Qin and Liu, 1982). A typical 3-fiber probe design is shown in Figure 2. The central fiber illuminates moving particles, while the outer fibers capture light reflected by the particles. For particles moving at constant speed in the direction connecting the two receiving fibers, the particle velocity, v_p, can be determined from

$$v_p = L_e/T_{AB}, \tag{4}$$

where L_e is the effective distance between A and B, and T_{AB} is the transit time. Note that L_e is, in general, not equal to the geometric distance between the axes of the two fibers.

There are two ways to measure T_{AB}. In cross-correlation (for example, Oki et al., 1975; Horio et al., 1988), T_{AB} is obtained from the time lag at which the cross-correlation function reaches a maximum. This method needs a sufficiently long integration time to give an accurate result. Previous authors (for example, Hartge et al., 1988; Herbert et al., 1994) used an integration time as short as 10 ms and generally no longer than 30 ms, except at the wall. The particle velocity obtained by cross-correlating signals for such short times can for most purposes be considered instantaneous. Oki et al. (1977) suggested that the transit distance, L_e, be no more than five particle diameters.

Another method, called the peak counting method, uses peak detectors to determine the time interval between successive peaks detected by fibers A and B. The fibers must be small enough to be able to detect the reflected light from individual particles. Zhou et al. (1995) employed a five-fiber-optical probe based on this method of measuring time−mean velocities of sand particles of mean diameter 213 μm in a circulating fluidized bed. However, because many data points are rejected as invalid, this method is unable to give continuous instantaneous velocities. Moreover, it gives the velocity of particles traveling in the direction of the vector connecting the receiving fibers, not the velocity component in that direction of all particles passing the probe.

Fiber-Optic Probe Design

Our novel probe combines concentration and velocity measurements, and then uses Eq. 1 to determine instantaneous values of $G_s(t)$. From the preceding analysis, peak counting is not well suited to give instantaneous particle velocities and solids concentrations. Therefore, for the concentration part, a type I probe, that is, of size > particle dimensions, was adopted, while particle velocities were determined by cross-correlation.

The probe configuration used in this work is similar to a regular velocity probe shown in Figure 2, with fiber diameter D_f and distance between two receiving fibers, L_p, carefully selected relative to the mean particle diameter. As discussed earlier, in order to measure instantaneous particle concentra-tion, D_f must be at least a few times bigger than the mean particle diameter. On the other hand, to guarantee a relatively good cross-correlation between the signals from fibers A and B, D_f and L_p cannot be too large.

A difficulty of this configuration is that, as shown in Figure 3, the parallel fibers may create a "blind zone," which falls either outside the region illuminated by the emission fiber or cannot be seen by the detection fiber. Particles moving through this blind zone tend to obscure those in the measurement volume, and this may give biased results. The extent of the blind zone is a function of the fiber size and spacing (Cui et al., 2001). Careful selection of fiber sizes and proper probe design are needed to obtain correct results, as discussed in the next section.

Several probes with different single-fiber diameter and/or distance between adjacent fibers were tested and compared. The probes, as well as signal conditioning components of the measuring system (see Figure 4), were fabricated by the Institute of Chemical Metallurgy in Beijing. The system includes an optical-fiber probe, light−voltage signal converter, signal preconditioning circuits, and a high-speed data-acquisition card whose speed can be as high as 2 MHz. A Pentium computer of speed 266 kHz and 64 MB memory acquired data and cross-correlated the signals.

Calibration of Local Particle Concentration

Theoretical analysis

Although optical probes are widely used in circulating fluidized beds, and various calibration equations have been employed, few previous investigators have considered the probe performance at a fundamental level. Several rigorous models can be found in the literature (Amos et al., 1996; Lischer and Louge, 1992). This study adopts a simplified approach similar to that suggested by Rensner et al. (1993), but adopts a different distribution function of power and applies the analysis to a multiple-fiber probe rather than a single-fiber probe (SFR). The model serves as a guide to the design and calibration of the novel multifunctional optical-fiber probe, and helps explain the calibration results.

Consider a two-fiber optical probe, with one fiber projecting light into a medium where there is a reflective surface (such as a particle layer), and the other receiving reflected light from the surface, as shown in Figure 5. One can consider the surface to be an ideal diffuse planar surface of diameter much bigger than the fiber-core diameter, normal to the fibers, at a distance x from their tips. The fraction of light reflected by the planar surface reaching the second fiber face is a function of x. The relationship, often called the reflective function, can be calculated if the fiber size and medium optical properties are known.

For simplicity, we ignore light losses, including losses inside the fiber and en route to and from the reflective surface through air (surrounding medium). The transmitted light leaves the projecting fiber within a maximum angle of
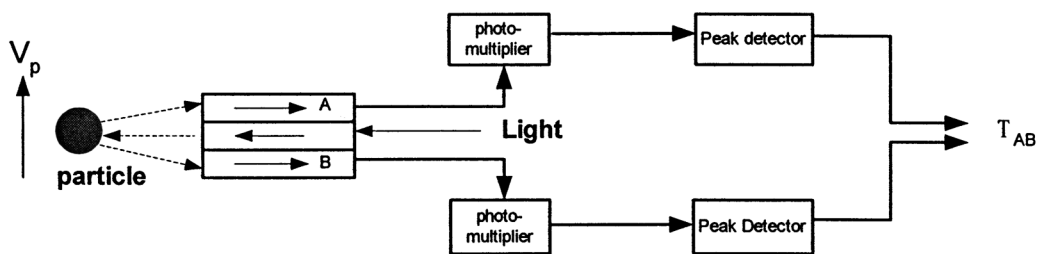
$$\theta_m = \arcsin\left(A_n/n_g\right) \tag{5}$$

where A_n is the numerical aperture of the fiber and n_g is the refractive index of the gas. For our fibers in air, our measurements show that θ_m can be taken as 30°.
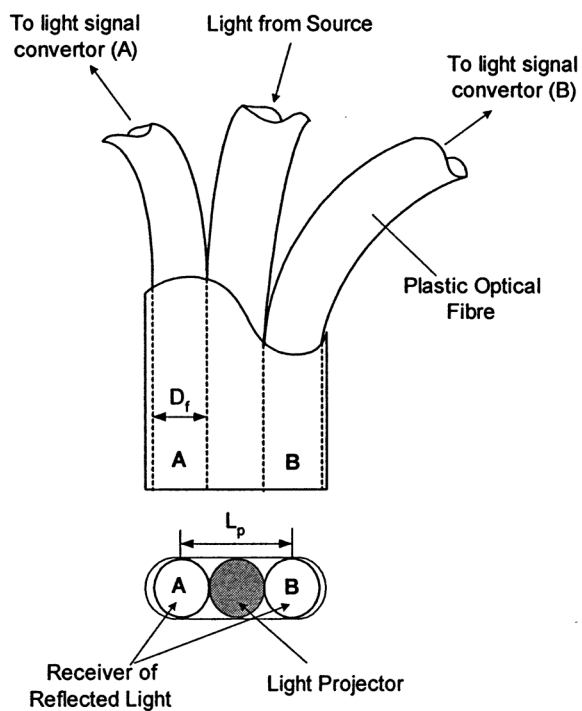
(a) Details of a typical 3-fiber velocity probe
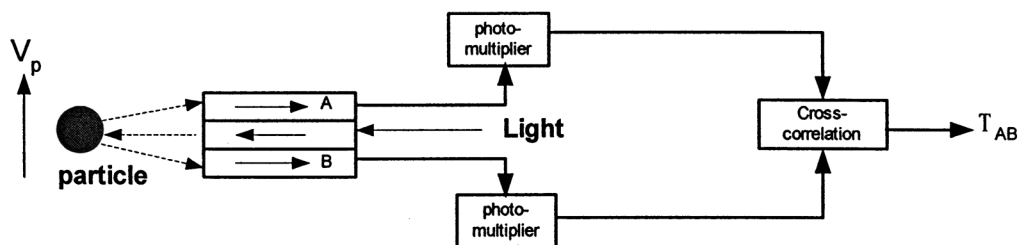
(b) Cross-correlation method

(c) Peak counting method

Figure 2. Fiber-optic probe and two signal-processing methods to obtain particle velocity (or particle transit time T_{AB} between two detecting fibers).
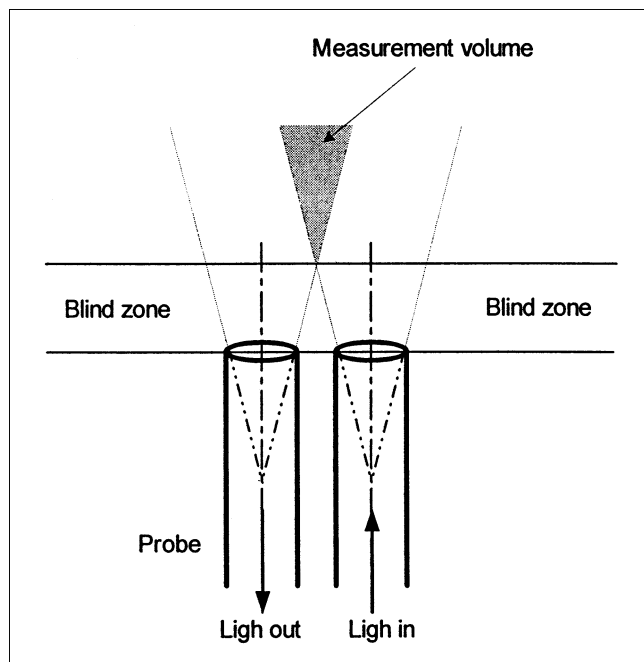
Figure 3. Measurement volume and "blind zone" for a parallel fiber pair.

The radiant intensity distribution of a fiber can usually be assumed (see Lischer and Louge, 1992) to be of Gaussian form

$$I(\theta) = K \exp \frac{-4\theta^2}{\theta_m^2} \qquad (6)$$

The constant K depends on the light itself, the fiber, and the probe geometry. It is independent of the light-emission angle θ. Although the light-intensity distribution on a plane surface at distance x is also affected by power transmission losses due to Fresnel reflection (Hardy and Perrin, 1932), such losses are ignored here. K can be calculated by specifying the total energy E_t emitted by the fiber. For simplicity, we set I equal to zero when $\theta > \theta_m$. For the surface at a distance $2x$ (see Figure 5) from the fiber face

$$E_t = \int_0^{\theta_m} K \exp\left(-\frac{4\theta^2}{\theta_m^2}\right)$$
$$\times 2\pi(R_{2x}\cot\theta_m)\tan\theta(1+\tan^2\theta)(R_{2x}\cot\theta_m)\,d\theta \quad (7)$$

so that

$$K = \frac{E_t}{2\pi(R_{2x}\cot\theta_m)^2\int_0^{\theta_m}\exp\left(-\frac{4\theta^2}{\theta_m^2}\right)\tan\theta(1+\tan^2\theta)\,d\theta} \qquad (8)$$

where R_{2x} is the radius of the light circle at a distance of $2x$ from the probe tips, that is, $R_{2x} = R_f + 2x\,\tan(\theta_m)$.

The total power captured by the receiving fiber is

$$E_i = 2\int_{r_a}^{r_b}\int_0^{\varphi_c} I(\theta)r\,d\varphi\,dr \qquad (9)$$

or, formulated as a power ratio

$$P_i = \frac{E_i}{E_t} = \frac{\tan^2\theta_m}{\pi R_{2x}^2}$$
$$\int_a^{r_b}\int_0^{\varphi_c}\frac{\exp\left(-\frac{4\theta^2}{\theta_m^2}\right)}{\int_0^{0_m}\exp\left(-\frac{4\theta^2}{\theta_m^2}\right)\tan\theta(1+\tan^2\theta)\,d\theta}r\,d\varphi\,dr \quad (10)$$

From the geometry

$$\varphi_c = \cos^{-1}\left(\frac{L_f^2 + r^2 - R_f^2}{2L_fR_f}\right) \qquad (11)$$

Referring to Figure 5, the integration limits r_a and r_b are written

$$R_{2x} \leq L_f - R_f \rightarrow \quad r_a = r_b = 0;$$
$$L_f - R_f < R_{2x} < L_f + R_f \rightarrow \quad r_a = L_f - R_f; \qquad r_b = R_{2x};$$
$$L_f + R_f < R_{2x} \rightarrow \quad r_a = L_f - R_f; \qquad r_b = L_f + R_f \quad (12)$$

Combining Eqs. 5–12, we can calculate probe reflective functions for various conditions and probe configurations.

Figure 6 presents the simulated reflective curves for optical-fiber probes of different single-fiber radii and different distances between a pair of fibers. The single-fiber radius shown in Figure 6a ranges from 10 μm to 500 μm, a range covering most fibers widely used in practice. The "power ratio" is the power of the light captured by the receiving fiber divided by that delivered by the projecting fiber. The emission and reception fibers are ideally arranged so that they are in contact with each other, with negligible wall thickness so that the distance between fiber centers, L_f, equals the single-fiber diameter. For probes with distinct light projection and detection fibers or fiber bundles, the reflective or response function is not monotonic. The power ratio first increases with increasing distance x_c then decreases beyond a certain distance, x_c, which increases both with fiber radius, R_f, and distance, L_f. From Figure 6a, it is possible to specify limits of the penetration depth. For $R_f = 100$ μm and $L_f = 200$ μm, the signal intensity falls below 10% of its maximum value at a distance of about 2 mm from the probe tip. This may be considered to represent the outer limit of the measuring volume of the probe.

Figure 6b shows that the light-intensity output decreases dramatically as the separation distance increases. For example, a change from $L_f = 200$ to 300 μm for a 200-μm-dia. single fiber causes more than a 50% decrease in the probe output. A low output probe may be adjusted by enlarging the
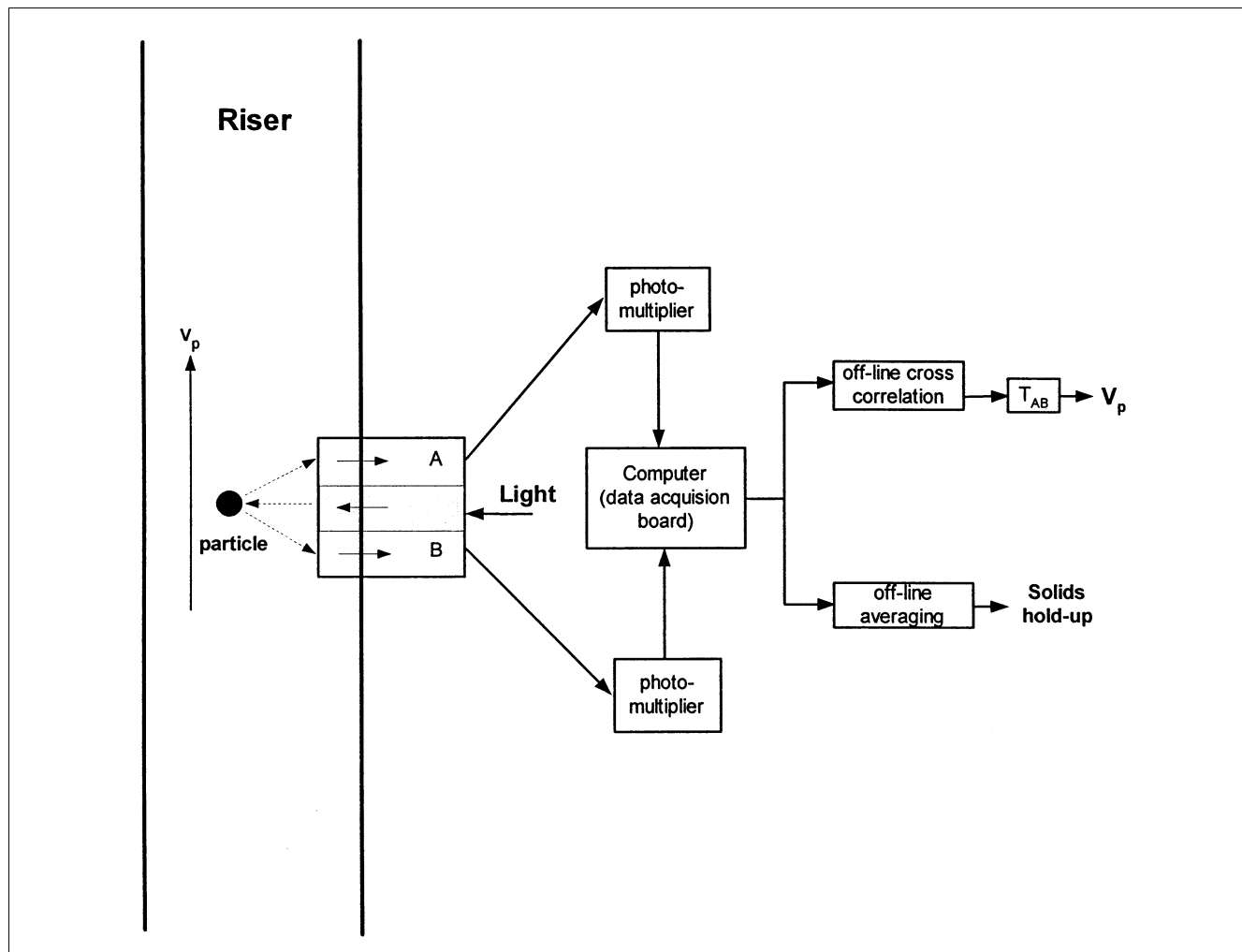
Figure 4. System to simultaneously measure local solids concentration and particle velocity.

signal amplification to compensate for the decrease in signal-to-noise level.

In order to measure local solids fraction precisely, a small measurement volume (but larger than the single-particle volume) is preferred. Multifiber probes provide practical solutions to this problem. In this type of probe, the individual fibers can be very small (such as 40 μm or less), with hundreds of fibers bundled together to view many particles.

Consider a gas–solids two-phase assembly of spherical particles, instead of the flat reflective surface. For spheres of diameter much greater than the wavelength of visible light, Deirmendjian (1969) noted that the scattered field can be estimated by tracing rays of light using classic laws of reflection and refraction at the interface, and considering the diffraction of rays by the sphere surface. Lischer and Louge (1992) believed that diffraction could be neglected for large spheres. For dense suspensions of opaque particles such as FCC, it is reasonable to assume that effectively any light incident on the surface of the packed bed will not penetrate more than one particle diameter into the bed. Only a tiny fraction of light penetrating into the bed deeper than one particle diameter is reflected back out of the bed (Amos et al., 1996).

Therefore the surface of a randomly packed bed of opaque particles can be considered a rough reflecting surface.

Gas–solids flowing suspensions can similarly be assumed to act as a reflecting surface, except that light penetrating deep into the bed can be reflected back only through void areas. If we ignore roughness effects, which cause multiple reflections in the cavities when the roughness is higher than the incident light wavelength, the gas–solids suspension can be considered as forming multiple flat smooth layers, with a distance of h_c between adjacent layers. Particles of diameter d_p are randomly arranged in each layer, and the thickness of each layer is equal to h_c.

We further assume that the power of light reflected by a surface layer is proportional to the projected area of particles in that layer, while the rest of the light passes through the surface toward the next layer. Power losses due to Fresnel reflection by each layer are again ignored. The reflective area is assumed to be equal to the projected area of particles.

To calculate the percentage of the projected area of particles, the solids volume fraction of each layer is treated as equal to the overall solids fraction, $1 - \epsilon$, and particles in each layer are assumed to be randomly distributed in space. For a
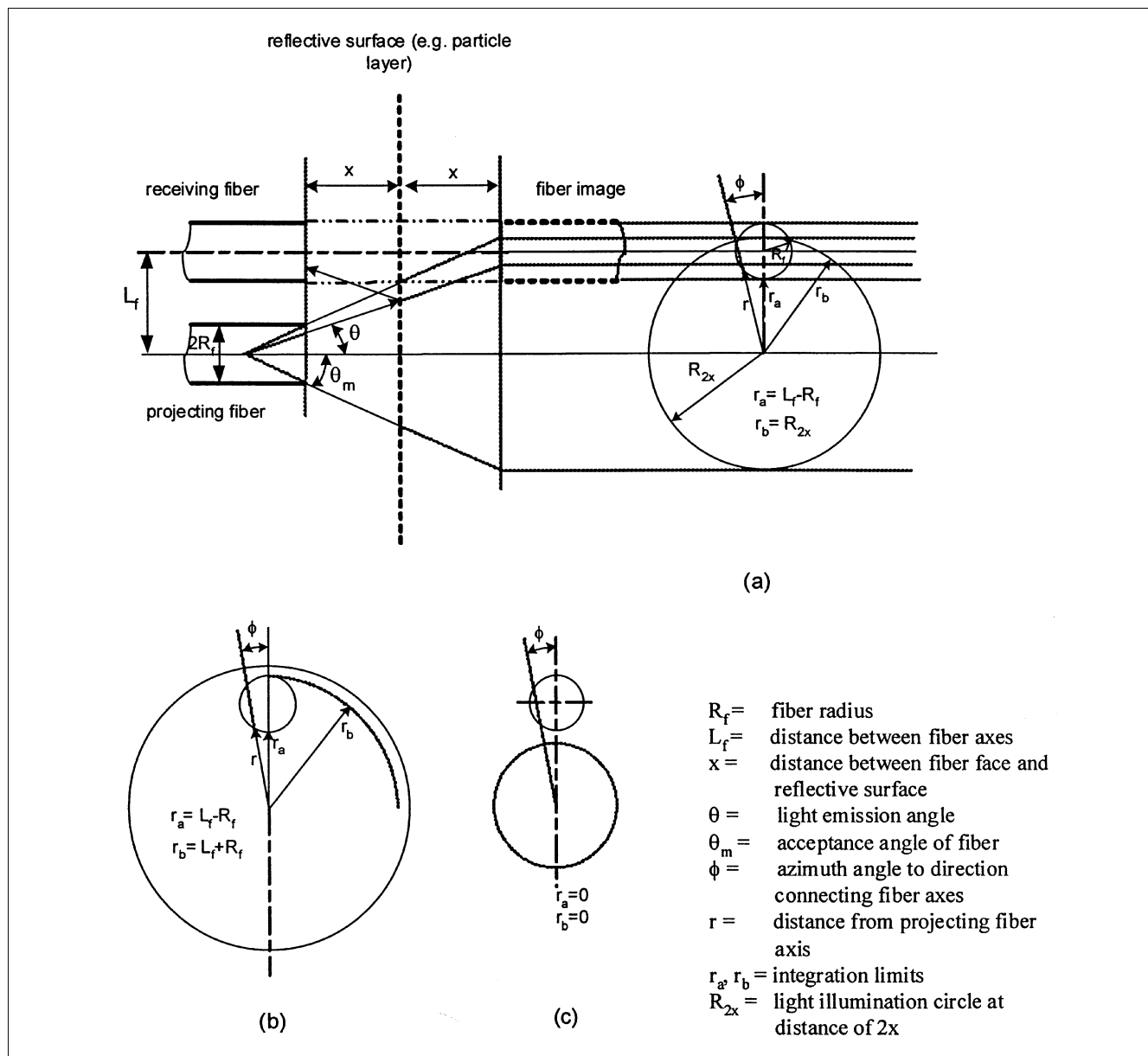
Figure 5. Fiber-optical probe with reflective surface (such as particle layer) at different distances from the probe tips: (a) $L_f - R_f < R_{2x} < L_f + R_f$; (b) $R_{2x} > L_f + R_f$; (c) $R_{2x} < L_f - R_f$.

sufficiently large volume containing M layers and N particles in each layer (where N and M are large integers), each layer can be assumed to be composed of N elementary cubes, with the side of each cube equal to h_c. As shown in Figure 7, the particle volume fraction is then given by

$$1 - \epsilon = \frac{NM\left(\frac{\pi}{6}d_p^3\right)}{NM(h_c^3)} = \frac{\pi}{6}\left(\frac{d_p}{h_c}\right)^3 \quad (13)$$

so that

$$h_c = \left(\frac{\pi}{6(1-\epsilon)}\right)^{1/3} d_p \quad (14)$$

Correspondingly, the fraction of the projected area occupied by particles is

$$\frac{A_p}{A_c} = \frac{\pi/4 d_p^2}{h_c^2} = \frac{\pi/4}{(\pi/6)^{2/3}}(1-\epsilon)^{2/3} = 1.209(1-\epsilon)^{2/3} \quad (15)$$

Let f be the percentage of light reflected back by each layer. For the first layer, $f_1 = f$. Light passing through the void area of the first layer reaches the second layer and some comes back again through the void area of the first layer. The fraction of light reflected by the second layer returning to the probe is
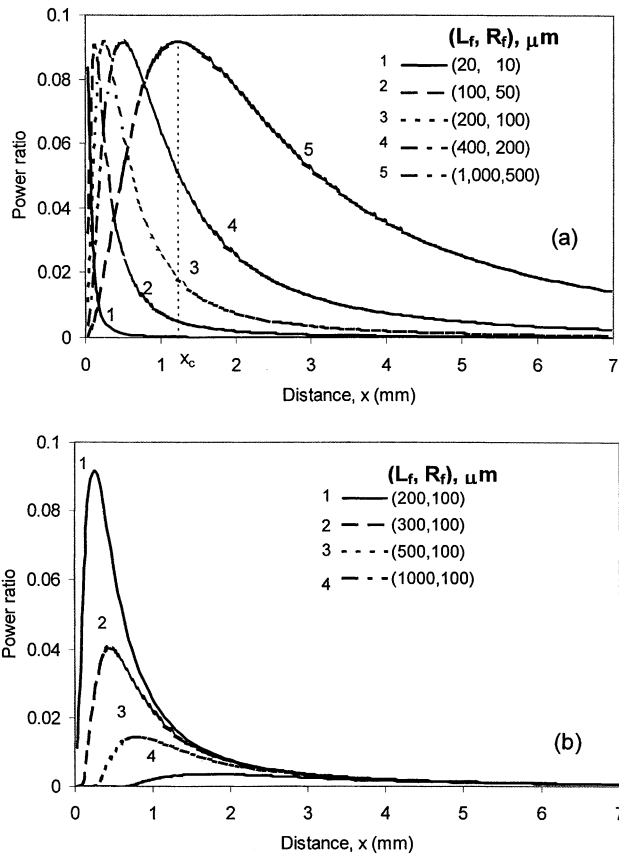
$$f_2 = (1-f)^2 f \quad (16)$$

Figure 6. **Reflective curves of two-fiber optical-fiber probes with: (a) different single-fiber diameters and fibers touching each other; (b) different distances between two fibers.**

Figure 7. **Simulated placement of particle matrix in front of optical-fiber probe.**
Dimensions are not to scale.

Similarly, for the ith layer

$$f_i = (1 - f)^{2(i-1)}f \qquad (17)$$

The total light intensity captured by the receiving fiber is the summation of the reflected light from all surface layers

$$P_t = \Sigma_i P_i(1-f)^{2(i-1)}f = \Sigma_i P_i\left(1 - \frac{A_p}{A_c}\right)^{2(i-1)}\left(\frac{A_p}{A_c}\right),$$
$$i = 1,2,3.\ldots \quad (18)$$

The distance from the ith layer to the fiber face is

$$x_i = (i - 0.5)h_c, \qquad i = 1,2,3.\ldots \quad (19)$$

Equation 18 is used to simulate calibration curves for a two-fiber (parallel-fiber) probe. Some results appear in Figures 8 and 9. The simulated calibration curves are nonlinear. In some cases, ambiguous signals or nonmonotonic calibration curves are obtained. For example, when $D_f \gg d_p$ (Figures 8a and 8b), or the distance between the projecting and detecting fibers is too great (Figure 8c), the calibration curves are highly nonlinear or even nonmonotonic, as reported by
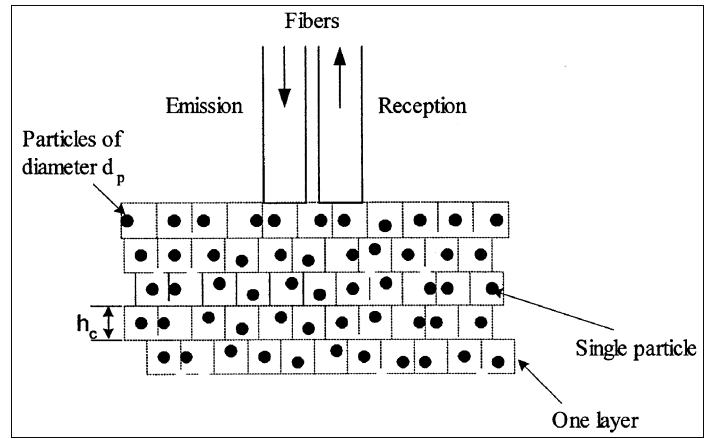
Rensner et al. (1991) and Reh and Li (1991). Probes with such calibration curves need careful and nonlinear calibrations, and, if nonmonotonic, may lead to error.

A linear calibration curve, where applicable, greatly simplifies the calibration procedure. According to our model, a monotonic or linear calibration curve can be obtained depending on the fiber sizes and/or the fibers' spatial arrangement. This has been confirmed experimentally. For similar optical probes (multifiber, $D_f = 40$ μm), He (1995) obtained a linear calibration function for glass beads ($d_p = 500$ μm), while Issangya (1998) found a nonlinear relationship for 70-μm FCC particles.

The different responses of these optical probes may be due to the "blind zone" (see Figure 3), and consequently to the nonmonotonic reflective function (Louge, 1997). To overcome this problem, Cocco et al. (1994) and Cui et al. (2001) suggest that a window thick enough to make the reflective curve monotonic be placed in front of the probe tip to eliminate this blind zone. Otherwise, the blind zone still exists, as confirmed in Figure 9. A properly designed protective window also makes the calibration curve nearly linear. In Figure 9a, for $D_f = 200$ μm and a protective window of thickness < 100 μm, the calibration curve is still nonlinear, but it approaches linearity when the window thickness is increased to 500 μm. For a smaller probe ($D_f = 80$ μm) in Figure 9b, a window of 80-μm thickness gives a nearly linear calibration curve.

The preceding analysis can be extended to multifiber optical probes. The multifiber parallel probe can be considered to be composed of many two-fiber probes, with the detected signal being the summation of the output from a large number of two-fiber probes having different distances between light emission and reception fibers. Given the detailed structure (number of fibers and their arrangement), the simulation can be carried out in a similar manner.

Results and discussion

The accuracy of concentration measurements depends on the design of the optical-fiber probe and the precision of the calibration. Measurements were obtained in this work using
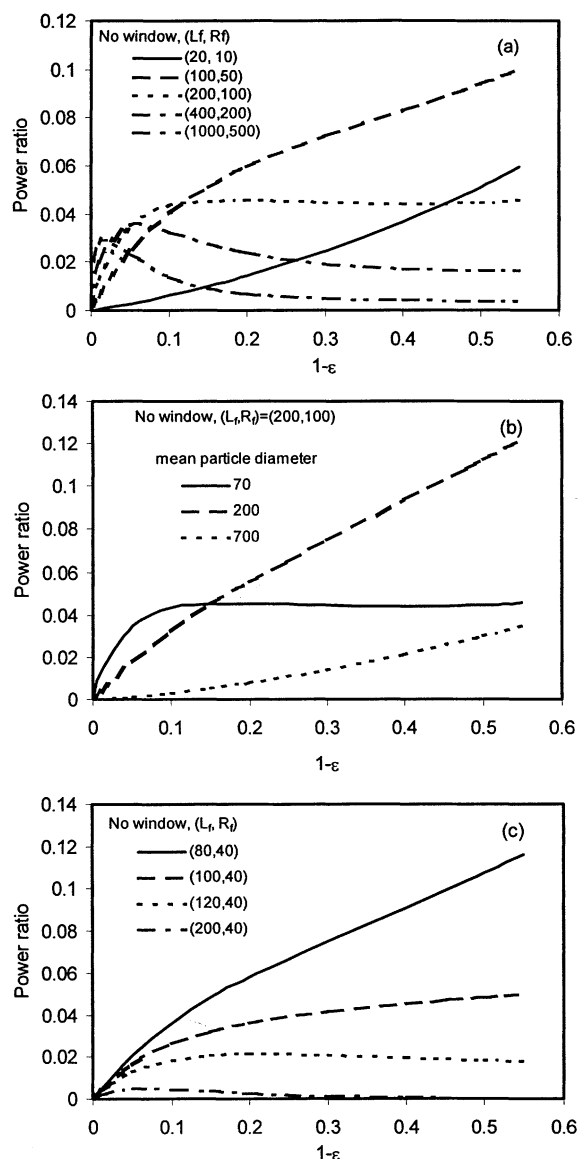
Figure 8. Simulated calibration curves for optical probe: (a) of different single-fiber size for FCC particles of diameter 70 μm; (b) for different particle diameters; (c) for different distances between fibers and FCC particles of diameter 70 μm.

L_f, R_f, and d_p are all in μm.

Figure 9. Simulated calibration curves for FCC particles using optical probes with glass windows of different thickness: (a) $R_f = 100$ μm; (b) $R_f = 40$ μm.

Thicknesses are in μm.

three probes, with configurations and sizes given in Figure 10. Since Probes I and II each contain two receiving fibers A and B (also known as Channels 1 and 2) and a single projecting fiber, an individual probe essentially acts as two similar separate two-fiber probes giving two distinct outputs. Their time-average values were virtually identical after properly adjusting the instrument gain and offset. Hence, for Probes I and II, only the results from fiber A (see Figure 4), that is, channel 1, are shown in Figures 11 to 14.

Probe Reflective Function. By recording the intensity of light reflected from dispersed FCC particles glued as a thick layer onto a black plate, and white paper, tests were per-
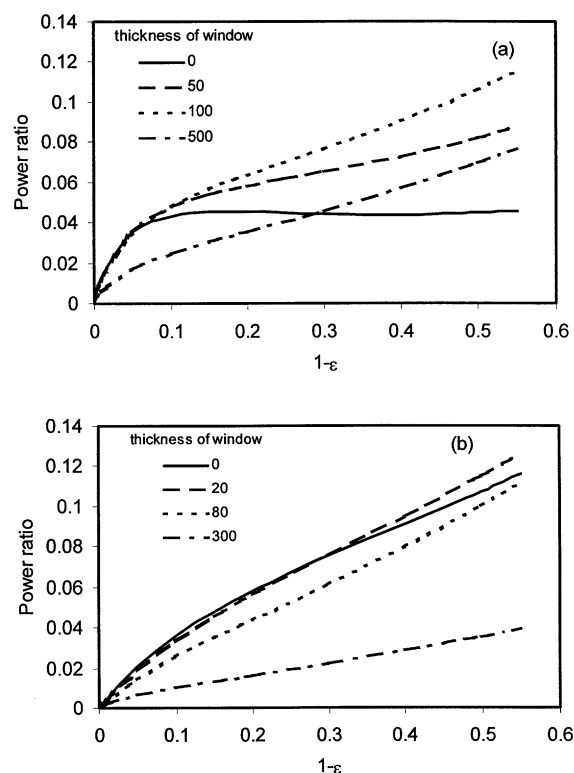
formed to determine the reflective curves and measurement volumes of the probes. In each case, the probe was traversed up and down, normal to the horizontal surface, to test the effect of the separation distance, x. Experimental results are shown in Figure 11 by the symbols, while the lines give the corresponding simulation curves. The probe output is expressed as the relative light intensity, that is, the light intensity divided by the maximum intensity at x_c. Different reflection surfaces give similar reflective curves, indicating that these three types of surface have similar reflective properties.

From Figure 11, the experimental limits of the penetration depths for probes I, II, and III beyond which the signal intensity fell below 10% of the maximum values are about 2, 15, and 8 mm, respectively. In gas–solids suspensions, the measuring volume at the probe tip decreases as the solids concentration increases, because the higher the particle concentration, the greater the shielding of more distant particles in the measuring volume. The actual measuring depth of Probe I should be less than 2 mm, usually small enough to be considered to give local measurements.

Probes I and II both had adjacent fibers in contact to give the shortest L_f. The single-fiber diameter then affects the measurement volume, consistent with our theoretical analysis. Although Probe III had the largest diameter (6 mm) of the three probes tested, its measurement depth was smaller than that of Probe II, because its single-fiber diameter was smaller ($D_f = 100$ μm). We would expect an even smaller

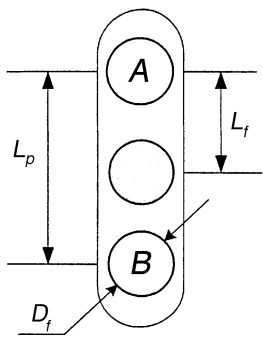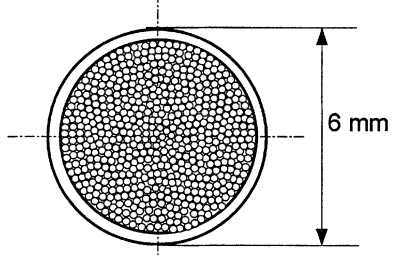| Name	Probe I	Probe II	Probe III
Probe type	3-fiber	3-fiber	multi-fiber
Structure of probe tip			Receiving and projecting fibers arranged in alternatating rows
Actual distance between centers of two receiving fibers L_p (mm)	0.53	2.0	N/A
Single fiber diameter D_f (mm)	0.26	1.0	~ 0.1

Figure 10. Dimensions of probes tested.

measurement depth for fibers of diameter 40 μm, this being a popular size for multifiber probes.

From Figure 11, it can be seen that our simulation agrees very well with the experimental results for both three-fiber Probes I and II. Given more details, such as the numbers of emission and detection fibers and their arrangements, it would be possible to perform the simulation for Probe III also. For concentration probes with pairs of fibers, smaller and well-defined measurement volumes are preferred. Hence, Probe I was chosen for further analysis and study.

Particle Concentration Calibration. Calibration methods may be classified as full and partial. Full calibrations are often performed with the help of quick-closing valves, which trap falling solids in a known volume surrounding the probe. Weighing the trapped solids allows the solids concentration to be determined for a series of suspension densities, leading to a full calibration curve. A partial calibration assumes that the nature of the calibration function between the solids concentration and voltage is known. If linearity is assumed, only two experiments are then needed (usually at the upper and lower limits) to fit the constants in the calibration equation. Alternatively, the commonly used approximate relationship between pressure drop and solids concentration

$$\frac{\overline{\Delta P}}{\Delta Z} \approx \left[\rho_p (1 - \epsilon) + \rho_g \epsilon \right] g \qquad (20)$$

can be used to estimate a cross-sectional average.

Full calibration should give a more reliable calibration. In this study, two units were used to calibrate our probes. The first was a dropping/trapping technique (Issangya, 1998), ex-

cept that the quick-closing valve was modified to make it easier to operate. The second involved a water−FCC suspension, using a well-stirred beaker. Since the refractive index of water is reasonably close to that of air, this method can give useful results, especially for near-linear calibration curves.

To eliminate the "blind zone" effect for Probe I, a quartz glass window of thickness about 0.5 mm was attached to the probe tip. This thickness exceeds x_c (0.18 mm for Probe I), and hence is enough to eliminate the blind zone and give a monotonic reflective curve, as shown in Figure 12. The fibers were in contact with each other.

Probe I was fully calibrated, both with and without the quartz glass window, using both calibration units. The results are compared with simulation predictions for $n = 1$ in Figures 13 and 14. Without the glass window, the calibration curves were highly nonlinear. They became almost linear with glass windows in place, consistent with our theoretical analysis. The simulations are in reasonable agreement with the experimental results, despite the different refractive indices. The calibrations in water and air give similar, but not identical, results. Other liquids, propanol and glycerine, with higher refractive indices than water are seen to make the calibration curves more nonlinear, suggesting that one should not directly apply calibrations obtained in liquids to calibrate probes for gas−solids systems. However, the results in liquid−FCC suspensions confirm the ability of the protective window to improve the linearity.

Local Particle Velocity Component

The local particle velocity is determined from the transit time T_{AB}, and the effective distance, L_e. The transit time T_{AB}
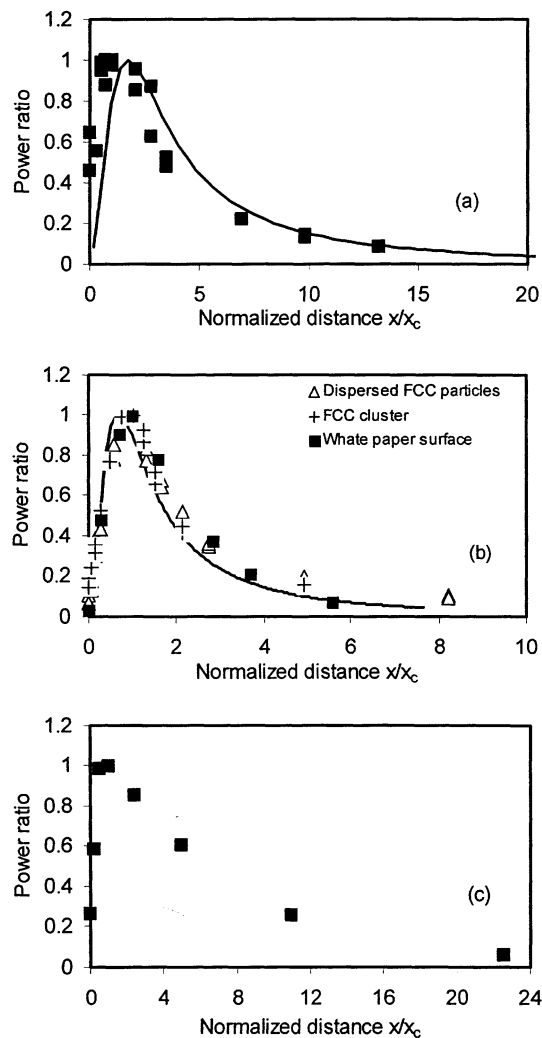
Figure 11. **Comparison of simulated and experimental reflective curves: (a) Probe I with dispersed 70-μm FCC on black plate; (b) Probe II with various surfaces; (c) multifiber Probe III with white paper.**

x_c for Probes I, II, and III are 0.18, 1.83, and 0.51 mm, respectively. For probe dimensions, see Figure 10. Points are experimental; lines simulation results.

can be calculated by cross-correlating the signals captured by fibers A and B, while determination of L_e requires careful calibration.

Cross-correlation technique

Figure 15 shows typical signals from two receiving fibers (channels) in the HDCFB riser. Due to the complex flow, irregular peaks and nonidentical signals were obtained from the two channels. It is therefore not suitable to use peak-detecting methods to determine the time delay. Cross-correlation provides the best means of finding T_{AB} and, hence, the particle velocity. The characteristic time delay, τ_m, can be defined by calculating the cross-correlation function of the two
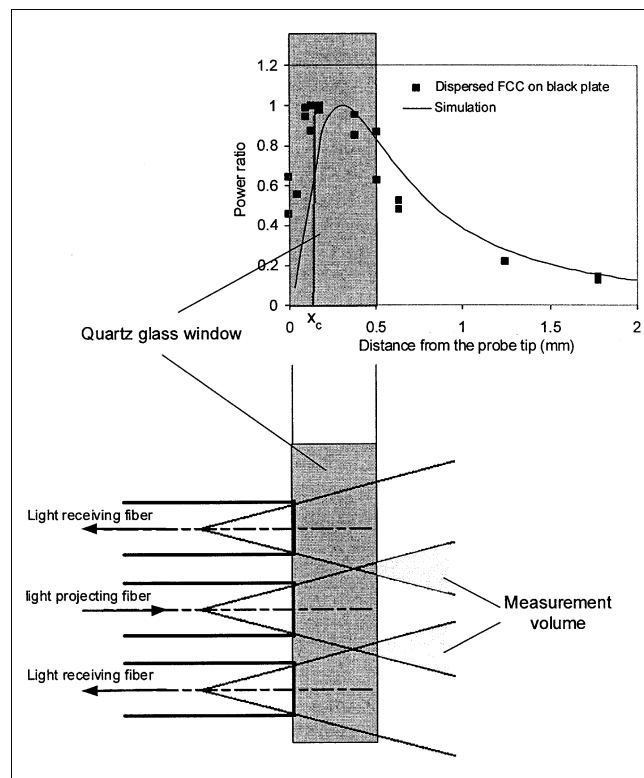

Figure 12. **Reflective curve and optical characteristics of Probe I with 0.5-mm-thick quartz glass window over the tip.**

signals, that is

$$\Phi_{I_1 I_2}(\tau) = \lim_{T \to \infty} \frac{1}{T} \int_0^T I_1(t) I_2(t + \tau)\, dt \qquad (21)$$

or the cross-correlation coefficient function (Herbert et al., 1994)

$$\rho_{I_1 I_2}(\tau) = \frac{\Phi_{I_1 I_2}(\tau) - \overline{I_1(t) I_2(t)}}{\sigma_{I_1} \sigma_{I_2}}, \qquad (22)$$

where $\overline{I_1(t)}$ and $\overline{I_2(t)}$ are the time-average signal intensities over time periods T, and σ_{I1} and σ_{I2} are the variances of the signals generated by two receiving fibers; τ_m is the time shift when the cross-correlation function takes a maximum value, corresponding to the average time of passage of flow structures between the two receiving fibers. In fluidized beds, particles may reverse directions, or a flow structure traveling nonvertically past one fiber may not be detected by the second fiber during the integration time, causing the cross-correlation coefficients to be low or indeterminate. Werther et al. (1996) only accepted data as valid for cross-correlation coefficients >0.6, causing 20−30% of their data to be discarded. Militzer et al. (1992) deleted data with correlation coefficients <0.5 or with calculated velocities differing by more than two standard deviations from the average. In our case, we reject data which do not give a single clear maximum or
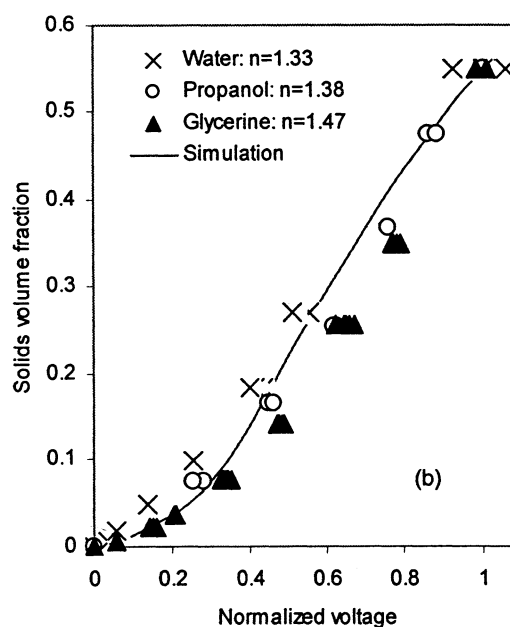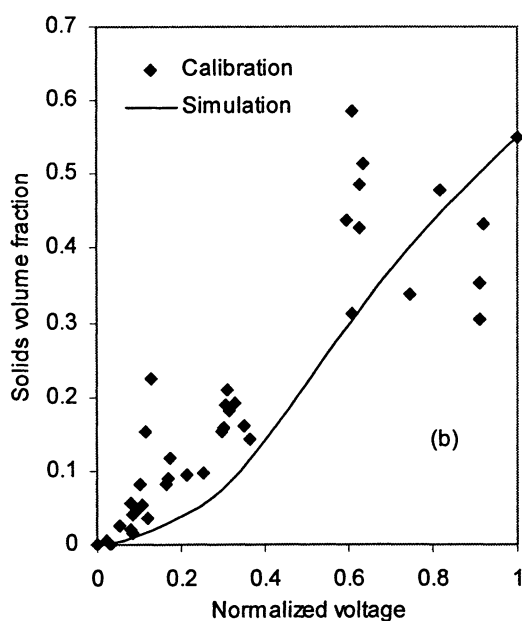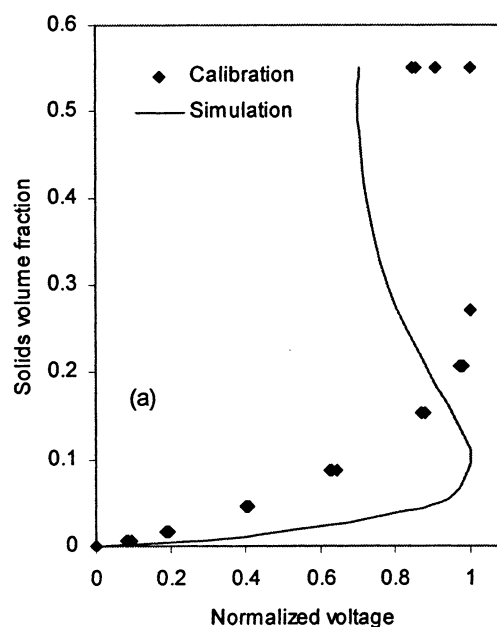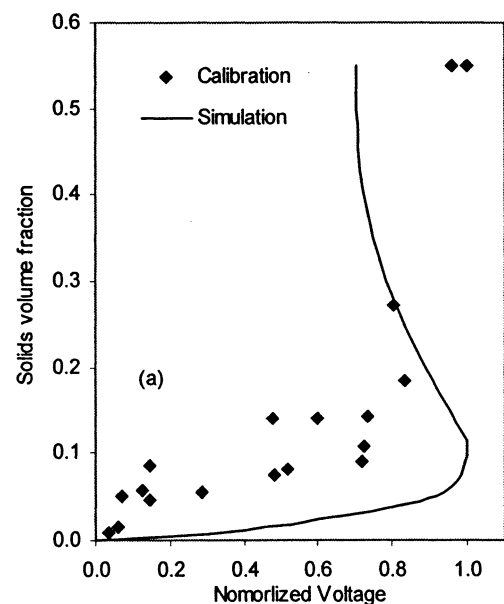
Figure 13. Comparison of simulated and experimental calibration curves for fiber optical probe with $L_p = 530$ μm, $D_f = 260$ μm, and 70-μm FCC particles in air using dropping/trapping technique: (a) without glass window; (b) with window of thickness 0.5 mm.

Figure 14. Comparison of simulated and experimental calibration curves for fiber-optical probe with $L_p = 530$ μm, $D_f = 260$ μm for 70-μm FCC particles: (a) without glass window in water–solids system; (b) with glass window of thickness 0.5 mm in liquids of different refractive index n.

that are negatively or insufficiently correlated. We also require that the correlation coefficients be greater than 0.5 and that the calculated velocities differ by no more than five standard deviations from the average.

In most CFB risers, particles mainly travel upward in the core and downward near the wall, exhibiting a core–annulus flow structure. Near the wall, the local instantaneous velocity can reverse directions. Hence, the characteristic time delay,

τ_m, can be negative when the solids descend if the upward direction is defined as positive.

Effective separation distance between fibers

To determine the particle velocity using Eq. 4, the effective distance, L_e, between receiving fibers A and B was deter-
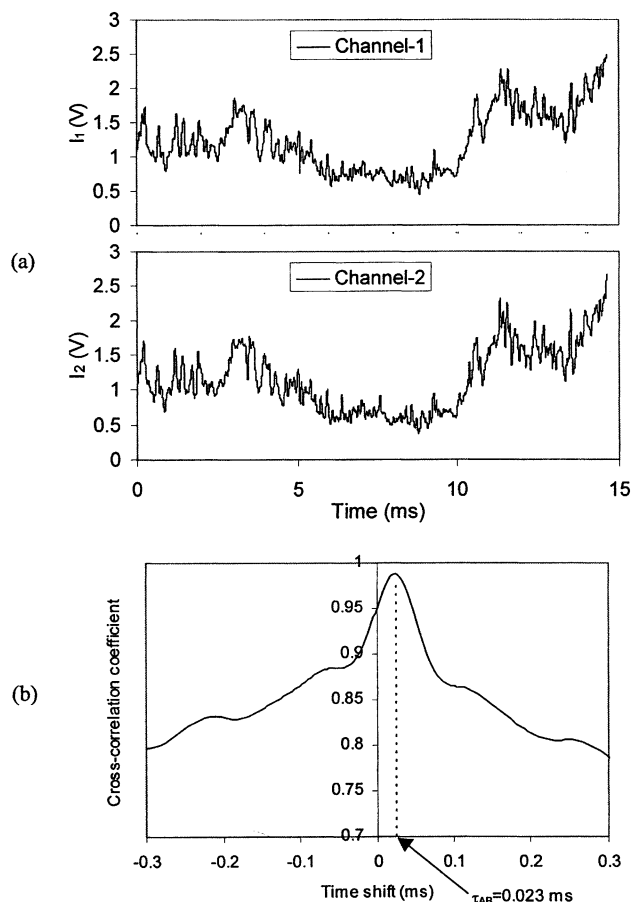
Figure 15. (a) Voltage waveforms for a period of 14.6 ms from measurements in the high-density CFB unit (Liu, 2001) with $U_g = 9$ m/s, $G_s = 485$ kg/m²s, and $z = 4.2$ m; (b) cross-correlation of these signals.

Maximum cross-correlation coefficient corresponds to time delay of 0.023 ms.
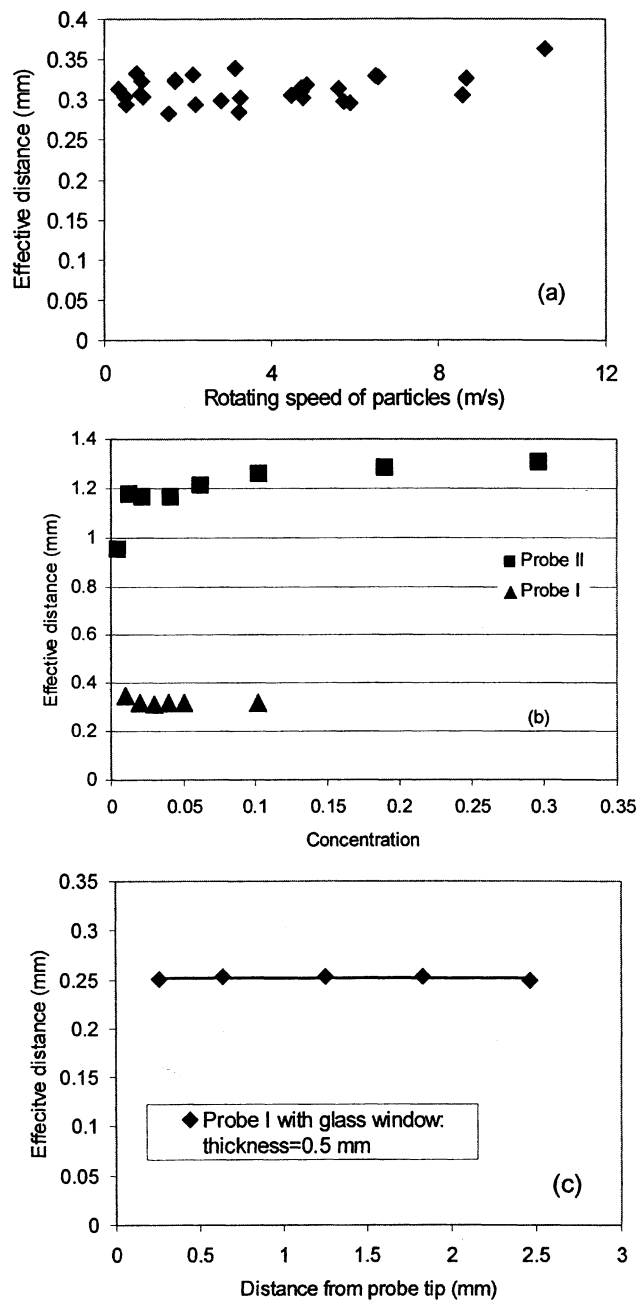

Figure 16. Calibration of effective fiber separation distance by (a) rotating disk method; (b) water–FCC suspension with FCC particles moving at 1.8 m/s; (c) Probe I with glass window at its tip for particle velocity of 0.44 m/s and sampling frequency 62.5 kHz.

mined by attaching one or more FCC particles to a rotating disk, recording the speed of rotation of the disk and then calculating the effective distance, L_e, using the cross-correlation method. The linear velocity was adjustable from 0.1 to 6 m/s, and the sampling frequency was 1–100 kHz. Results for Probe I without the glass window are plotted in Figure 16. L_e was found to be ∼0.31 mm, about half the geometric distance, L_p.

While the rotating-disk method is simple, it is not without problems. The rotating disk functions as a 2-D surface, while in the real measurements, the probe is inside a 3-D gas–solid suspension. Since the refractive indices for water and air are similar, the probe was also calibrated in a well-mixed water–FCC tank. The suspension was agitated to make it uniform, and therefore the local volumetric fraction of FCC can be calculated, since the mass and density of the particles and the volume of liquid added were all independently determined. The probe was placed very close to the edge of the agitator blade (within 5 mm), so that the FCC particles inside the measurement volume move at essentially the same angular speed as the stirrer blade. In this way, the effective dis-

tance of the probe was checked in a 3-D environment for different particle concentrations. From Figure 16b, the magnitude of L_e for Probe I is almost the same as from the rotating-disk method. Adding a thin glass window at the probe tip not only radically alters the solids concentration calibration and measurement, but also changes the effective distance, L_e, from ∼0.31 mm to 0.25 mm for Probe I, as shown in Figure 16c, probably due to refraction by the quartz glass window.

With τ_m and L_e known, the particle velocity can be calculated from Eq. 3. The lowest measurable absolute velocity is related to the integration time T. The maximum time delay τ_m cannot exceed $T/2$, with the particle velocity corresponding to this time delay being $|V_{min}| = 2*L_e/T$. No particle velocity can be measured less than this. For example, for Probe I with an integration time of 14.6 ms, the lowest measurable absolute particle velocity is 0.045 m/s. Any velocities with magnitudes below this value are considered to be 0. In fact, in CFB systems very few particles have velocity magnitudes less than this. Hence, any bias introduced by the inability of the probe to measure such small velocities is expected to be very small for most positions in the riser cross section. To minimize errors in the wall region where significant numbers of particles travel upwards and downwards with small speeds, a longer integration time of ~40 ms was used, further lowering the lowest measurable speed to 0.016 m/s. The effect on the measurement is then small, especially considering that some particles with speed <0.016 m/s will be moving upwards and some downwards.

High-speed data acquisition system

Since the cross-correlation is a discrete function of the time lag τ, determined as integral multiples of the sampling interval, significant error is introduced in the velocity calculation
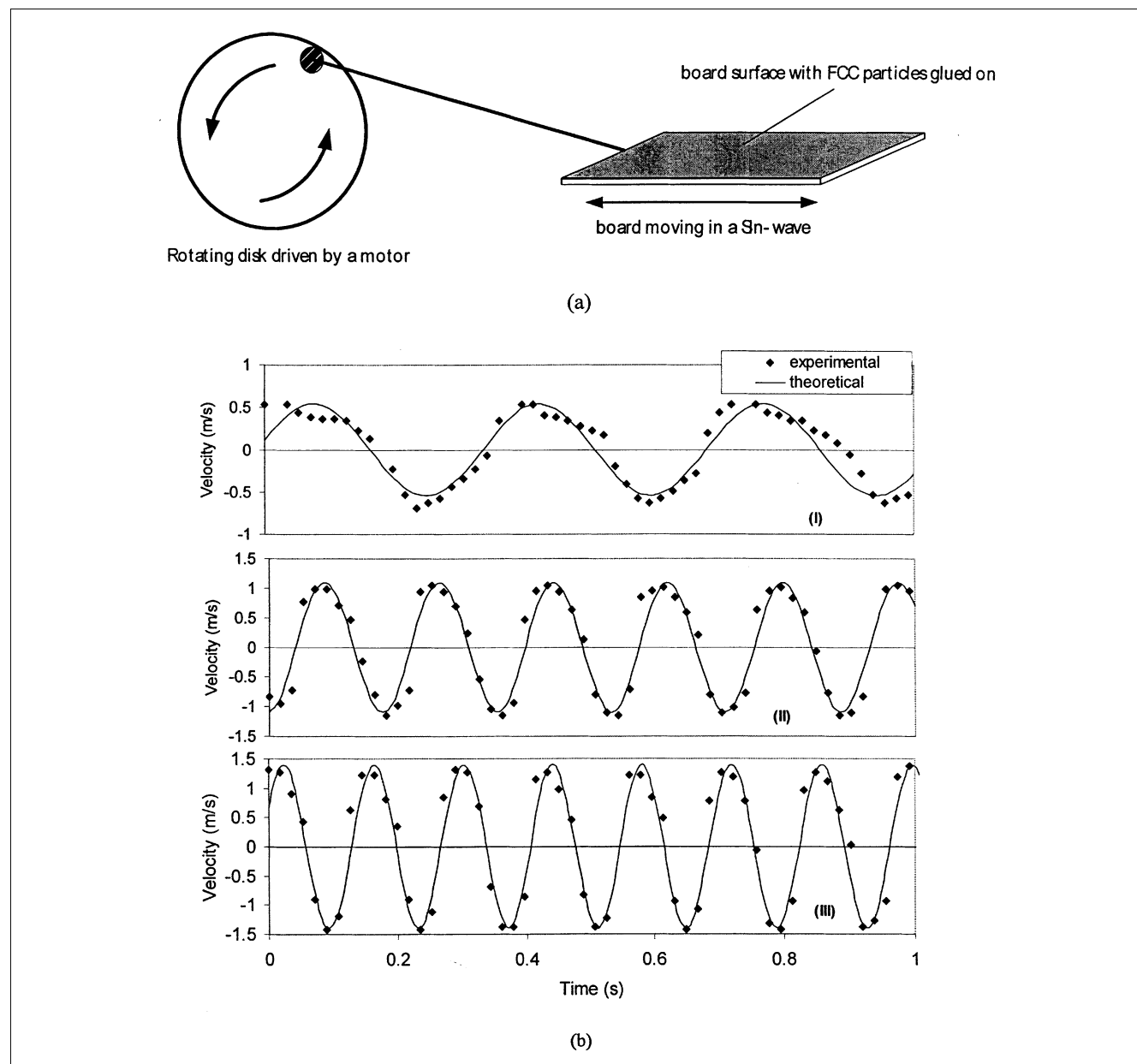

Figure 17. (a) Measurement device where FCC particles are glued on an oscillating surface; **(b)** FCC particle velocities measured using optical probe at different motor speeds: **(I)** 162, **(II)** 338, **(III)** 432 rpm.

$p = 0.2$, 4.8, and 0.5 for these three cases.

when few points are sampled during the passage of a particle between the two fibers. The error v_e defined as the difference in velocity calculated from two neighboring points around the time delay τ_m is directly related to the sampling frequency, f, the effective distance L_e between the receiving fibers and the particle velocity v_p (Herbert et al., 1994)

$$f = \frac{v_p(v_p - v_e)}{L_e v_e} \qquad (23)$$

The instantaneous solids velocity in CFB risers can exceed 10 m/s. A sampling frequency of 171 kHz is needed for a measurement error of 1.5 m/s (15%) with Probe I. For $\sim$30 s of continuous sampling for each velocity determination, a very large number of data ($\sim$40 MB) are required for each velocity determination. A high-speed data-acquisition system was developed (Liu, 2001) using the C programming language under the DOS operation system, allowing data to be acquired at up to 300 kHz for each channel. Cross-correlation to determine velocities and other data analysis (such as to calculate mean concentration or velocities) were performed off-line using Matlab software.

Accuracy of optical probe

To test the accuracy of the optical probe, FCC particles were glued onto a horizontal surface to form dispersed particles and clusters several particles thick. The surface was then connected, as shown in Figure 17a, by a stiff rod to the circumference of a rotating disk driven by an electrical motor whose speed could be adjusted from 0 to 600 rpm. The radius of the center of the end of the rod was 0.0305 m, so that the maximum velocity of the particles was 1.9 m/s. The particle velocities should then oscillate backward and forward, following a sinusoidal wave function, with

$$v_p = 2\pi r f \sin(2\pi f t + p) \qquad (24)$$

where r is the radial position of the end of the rod, f is the frequency of rotation and p is a phase-shift factor obtained by fitting.

Particle velocities were measured by the optical probe normal to the board surface. Signals were recorded for a duration of 5 s and cross-correlated to calculate time lags and instantaneous velocities, as discussed earlier. The rejection rate (percentage of invalid particle velocities) was $< 5\%$. Figure 17b shows velocity distributions for three motor speeds —162, 338, and 432 rpm—corresponding to maximum velocities of 0.52, 1.1, and 1.4 m/s. The points represent experimental values measured by the optical probe, while the curves are from Eq. 24. The good agreement between the experimental data and predications confirms the ability of the optical probe to measure time-varying particle velocities accurately, even under reversing conditions.

Conclusions

A parallel 3-fiber optical probe was developed to simultaneously determine local instantaneous solids volume concentration, velocity and flux in multiphase suspensions. The central fiber projects light into the gas−solids suspensions, while two adjacent fibers receive backscattered light from moving particles. The backscattered light is then converted to voltage waveforms, which vary with time and are recorded by a high-speed data-acquisition system. Local instantaneous velocities are determined by cross-correlating the waveforms from the two receiving fibers over a time of 10−40 ms, finding the time lag at which the cross-correlation function reaches a maximum, and dividing into the effective separation distance L_e, calibrated experimentally.

A simple mechanistic model explains the existence of a "blind zone" and successfully predicts the reflective and calibration results for probes of different size. It also shows the influence of such variables as the single-fiber diameter and distance between adjacent fibers. Covering the front of the probe tip with a quartz glass window can dramatically improve the concentration calibration function to nearly linear, facilitating the measurement of solids volume fraction. The local instantaneous solids flux can then be calculated by multiplying the local instantaneous suspension density by the simultaneously determined local instantaneous particle velocity.

Notation

A_n = numerical aperture of optical fiber
A_p = projected area of particle, m^2
D_f = single-fiber diameter, m
E = energy emitted by fiber, J/s
f = sampling frequency (Hz) or percentage of light reflected by particle layer
f_i = fraction of light reflected by ith particle layer
G_s = cross-sectional average solids circulation flux, kg/m$^2 \cdot$s
$\overline{G_s}$ = time-mean local solids flux, kg/m$^2 \cdot$s
$G_s(t)$ = instantaneous local solids flux, kg/m$^2 \cdot$s
$I, I(t)$ = electrical signal corresponding to instantaneous voidage, V
$I(\theta)$ = radiant intensity of fiber, J/(sm^2)
K = constant in Eqs. 6−8, J/(sm^2)
L_e = effective transit distance of optical-fiber probe, m
L_f = distance between axes of two adjacent fibers, m
L_p = distance between axes of two receiving fibers, m
n = refractive index
r = radial coordinate, m
r_a, r_b = radii shown in Figure 5, m
R_f = radius of fiber, m
t = time, s
T = cross-correlation integration period, s
T_{AB} = transit time between fibers A and B, s
U_g = superficial gas velocity, m/s
v_E = measurement error of particle velocity, m/s
$v_p, v_p(t)$ = instantaneous local particle velocity, m/s
$\overline{v_p}$ = time-mean local particle velocity, m/s
x = distance from end of optical fiber, m
x_c = critical distance, m
z = vertical coordinate measured from bottom of CFB riser, m

Greek letters

ΔP = pressure difference, kPa
ΔZ = vertical distance between two pressure transducers, m
$\epsilon(r), \epsilon$ = instantaneous local voidage
$\bar{\epsilon}$ = time-mean local voidage
ϵ_m = riser cross-sectional average voidage
$\Phi_{I_1 I_2}(\tau)$ = cross-correlation function

$\rho_{I_1 I_2}(\tau)$ = cross-correlation coefficient
τ = time shift, s
θ_m = acceptance angle of optical fibers

Subscripts

1,2 = data-acquisition Channel 1, 2
g = gas
p = particle

Literature Cited

Amos, G., M. J. Rhodes, and H. Benkreira, "Calculation of Optic Fibres Calibration Curves for the Measurement of Solids Volume Fractions in Multiphase Flows," *Powder Technol.,* **88**, 107 (1996).

Bao, J., R. E. Van de Wall, and S. L. Soo, "Simultaneous Use of LDV and PDPA on Particle Suspensions," *Circulating Fluidized Bed Technology,* Vol. V, M. Kwauk and J. Li, eds., Preprint, MI3 1-6 (1996).

Bi, H. T., J. Zhou, S. Z. Qin, and J. R. Grace, "Annular Wall Layer Thickness in Circulating Fluidized Bed Risers," *Can. J. Chem. Eng.,* **74**, 811 (1996).

Chrisman, R., R. Cocco, and J. Cleveland, "Method and Apparatus for Determining Flow Rates and Concentrations in Multi-Phase Streams," U.S. Patent No. 5,365,326 (1994).

Cocco, R., J. Cleveland, R. Harner, and R. Chrisman, "Simultaneous In-Situ Determination of Particle Loading and Velocities in a Gaseous Medium," *AIChE Symp. Ser.,* **91**(308), 147 (1994).

Cui, H., N. Mostoufi, and J. Chauki, "Comparison of Measurement Techniques of Local Particle Concentration for Gas-Solid Fluidization," *Fluidization X*, M. Kwauk, J. Li, and W. C. Yang, eds., Engineering Foundation, p. 779 (2001).

Deirmendjian, D., *Electromagnetic Scattering on Spherical Polydispersions*; Elsevier, New York (1969).

Hardy, A. C., and F. H. Perrin, *The Principles of Optics*, McGraw-Hill, New York (1932).

Hartge, E. U., D. Rensner, and J. Werther, "Solids Concentration and Velocity Patterns in Circulating Fluidized Beds," *Circulating Fluidized Bed Technology,* Vol. II, P. Basu and J. F. Large, eds., Pergamon, Oxford, p. 165 (1988).

He, Y. L., "Hydrodynamics and Scale-Up Studies in Spouted Beds," PhD Diss., The Univ. of British Columbia, Vancouver, BC, Canada (1995).

Herb, B., K. Dou, K. Tuzla, and J. C. Chen, "Solids Mass Fluxes in Circulating Fluidized Beds," *Powder Technol.,* **70**, 215 (1992).

Herbert, P. M., T. A. Gauthier, C. L. Briens, and M. A. Bergougnou, "Application of Fiber Optic Reflection Probes to the Measurement of Local Particle Velocity and Concentration in Gas-Solid Flow," *Powder Technol.,* **80**, 243 (1994).

Horio, M., K. Mori, Y. Takei, and H. Ishii, "Simultaneous Gas and Solid Velocity Measurements in Turbulent and Fast Fluidized Beds," *Fluidization,* Vol. VII, O. E. Potter and D. J. Nicklin, eds., Engineering Foundation, New York, p. 756 (1991).

Issangya, A. S., "Hydrodynamics of a High-Density Circulating Fluidized Bed," PhD Thesis, The Univ. of British Columbia, Vancouver, B.C., Canada (1998).

Kallio, S., "Simultaneous Measurement of Local Porosities and Solids Velocities in a CFB Riser," *Circulating Fluidized Bed Technology,* Vol. V, M. Kwauk and J. Li, eds., Science Press, Beijing, p. 639 (1996).

Krohn, D. A., Soc. Photo-Optical Instr. Engrs. *(SPIE),* Vol. 718, *Fiber Optics and Laser Sensors IV*, p. 2 (1986).

Lischer, J. D., and M. Y. Louge, "Optical Fiber Measurements of Particle Concentration in Dense Suspensions: Calibration and Simulation," *Appl. Opt.,* **31**, 5107 (1992).

Liu, J., "Particle and Gas Dynamics of High Density Circulating Fluidized Beds," PhD Diss., The Univ. of British Columbia, Vancouver, BC, Canada (2001).

Louge, M., "Experimental Techniques," *Circulating Fluidized Beds,* Chap. 9, J. R. Grace, A. A. Avidan, and T. M. Knowlton, eds., Chapman & Hall, London (1997).

Militzer, J., J. P. Hebb, G. Jollimore, and K. Shakourzadeh, "Solid Particle Velocity Measurements," *Fluidization,* Vol. VII, O. E. Potter and D. J. Nicklin, eds., Engineering Foundation, New York, p. 763 (1992).

Oki, K., W. P. Walawender, and L. T. Fan, "The Measurement of Local Velocity of Solid Particles," *Powder Technol.,* **18**, 171 (1977).

Oki, K., T. Akehata, and T. Shirai, "A New Method for Evaluating the Size of Moving Particles with a Fiber Optic Probe," *Powder Technol.,* **11**, 51 (1975).

Qin, S., and D. Liu, "Application of Optical Fibers to Measurement and Display of Fluidized Systems," *Fluidization '82: Science and Technology,* M. Kwauk and D. Kunii, eds., Science Press, Beijing, p. 258 (1982).

Reh, L., and J. Li, "Measurement of Voidage in Fluidized Beds by Optical Probes," *Circulating Fluidized Bed Technology,* Vol. III, P. Basu, M. Horio, and M. Hasatani, eds., Pergamon, Oxford, p. 163 (1991).

Rensner, D., and J. Werther, "Estimation of the Effective Measuring Volume of Single-Fibre Reflection Probes for Solid Volume Concentration Measurements," *Part. Part. Syst. Character.,* **10**, 48 (1993).

Rensner, D., E. U. Hartge, and J. Werther, "Different Types of Optical Probes for Investigations in Highly Concentrated Gas/Solid Flows," *Proc. Int. Conf. on Multiphase Flows,* G. Matsui, A. Serizawa, and Y. Tsuji, eds., Tsukuba, Japan, p. 255 (1991).

Werther, J., B. Hage, and C. Rudnick, "A Comparison of Laser Doppler and Single-Fibre Reflection Probes for the Measurement of the Velocity of Solids in a Gas-Solid Circulating Fluidized Bed," *Chem. Eng. Process.,* **35**, 381 (1996).

Zhou, J., J. R. Grace, C. J. Lim, and C. Brereton, "Particle Velocity Profiles in a Circulating Fluidized Bed of Square Cross-Section," *Chem. Eng. Sci.,* **50**, 237 (1995).